Pol. J. Environ. Stud. Vol. XX, No. X (XXXX), 1-16

DOI: *10.15244/pjoes/220958* ONLINE PUBLICATION DATE: 2026-09-10

Original Research

Regional Disparities and Spatiotemporal Evolution of Non-Point Source Pollution Loads from Crop Straw Fertilizer Utilization in China under Rural Revitalization

Hongmei Huo[1], Qi Qi[1], Weibo Zhang[2], Zheng Liu[3]*

[1]Party School of the Liaoning Provincial Committee of the Communist Party of China, Shenyang, 110004, China
[2]College of Economics, Southwestern University of Finance and Economics, Chengdu 611130, China
[3]Liaoning Academy of Agricultural Sciences, Shenyang, 110161, China

Received: 11 January 2026
Accepted: 21 April 2026

Abstract

Crop straw recycling as organic fertilizer is widely promoted in China to curb open burning and enhance nutrient cycling, yet its potential contribution to agricultural non-point source pollution remains insufficiently quantified. Using provincial panel data for 31 regions during 2017-2024, this study estimates pollution loads associated with crop straw fertilizer utilization, focusing on total nitrogen (TN), total phosphorus (TP), and chemical oxygen demand (COD). Nationally, TN, TP, and COD loads show a mild but persistent increase over the study period, with COD contributing the largest share. Dagum Gini decomposition indicates that interprovincial inequality is substantial and relatively stable, and that between-region differences account for most of the overall disparity, while within-region inequality is particularly pronounced in the eastern region. Kernel density estimation suggests a consistently right-skewed distribution, with most provinces remaining at low load levels but a small set of provinces forming a high-load tail that becomes slightly more prominent in recent years. Global Moran's I is positive but statistically insignificant, implying weak nationwide spatial clustering; however, local indicators of spatial association reveal stable hotspot and coldspot provinces. Spatial Markov analysis further shows strong state persistence, while high-neighborhood contexts are associated with more active transitions between higher-load states. Policy implications emphasize integrated straw management and regionally differentiated control strategies.

Keywords: crop straw recycling, fertilizer utilization, agricultural non-point source pollution, Dagum Gini decomposition, spatial Markov chain

*e-mail: liuzheng@laas.cn
0009-0006-8032-5404

Introduction

China is a major producer of crop straw, contributing nearly 18% of global output annually [1]. For many years, limited utilization pathways led to widespread open-field burning, causing both resource waste and severe air pollution [2]. From an environmental perspective, returning straw to farmland as organic fertilizer and promoting circular use of straw resources are important for improving the rural ecological environment [3]. Because straw contains substantial plant nutrients, its fertilizer utilization can partially substitute chemical fertilizers and reduce agricultural non-point source pollution at the source. Evidence suggests that if all usable nutrients in crop straw were used to replace chemical fertilizers, average nitrogen and phosphorus losses in Chinese agriculture could decrease by about 55% and 65%, respectively [4]. Therefore, crop straw fertilizer utilization is highly relevant because it can simultaneously promote agricultural residue recycling and non-point source pollution mitigation.

The environmental effects of straw incorporation have been widely studied. Existing assessments show that straw return can improve soil fertility, increase crop yields, and help reduce nutrient-loss-related environmental pollution [5]. Field experiments also indicate that long-term straw incorporation can reduce nitrogen losses in farmland runoff. For example, in rice-based systems, long-term straw return reduced total nitrogen losses in surface runoff by 2.3%-26.1%, mainly by increasing soil organic matter and nutrient retention, thereby reducing inorganic nitrogen loss [6]. Nutrients released during straw decomposition can also be reabsorbed by crops, reducing fertilizer demand and the risk of nutrient surplus. Wang et al. emphasized that straw return has become an important substitute source of fertilizer nutrients, and many empirical studies show that it can reduce both chemical fertilizer use and soil nutrient loss risk [7]. Overall, well-managed crop straw fertilizer utilization is widely regarded as an environmentally friendly agronomic practice that improves soil fertility while lowering non-point source pollution loads.

Agricultural non-point source pollution has long threatened China's water environment, and its spatiotemporal dynamics have attracted growing attention. Xu et al. reported that about 40% of major pollutants in Chinese waters originate from agricultural non-point sources, and that emissions of COD, TN, and TP have reached several million tons with an upward trend [8]. The problem is especially serious in major grain-producing regions, where eutrophication in rivers and lakes has intensified and agricultural non-point source pollution has become a major ecological pressure [9]. One key driver is excessive agricultural chemical input. Since the 1990s, fertilizer and pesticide use in China has increased rapidly; from 1991 to 2008, chemical nitrogen fertilizer application rose by more than 50%, and surplus nitrogen and phosphorus were transported into water bodies through runoff, accelerating deterioration such as lake eutrophication [10]. Influenced by unreasonable fertilization and livestock and poultry waste discharges, about half of China's major lakes in the early 21st century experienced eutrophication to varying degrees [10]. In recent years, however, policies on fertilizer and pesticide reduction and non-point source pollution control have partly curbed growth in some areas, and signs of a turning point have emerged [11]. For example, evidence from the Huang–Huai–Hai Plain shows that total agricultural non-point source pollution emissions increased during 2000-2015 but declined slightly after 2015 [9]. These changes underscore the need for an updated national-scale assessment.

To better understand regional environmental problems such as agricultural non-point source pollution, spatial analytical tools have been increasingly used to identify spatial heterogeneity and patterns of evolution. Global and local Moran's I are widely used to detect clustering of high- and low-value areas [12]. Hu et al. found significant positive spatial correlation in agricultural non-point source pollution at the provincial scale in China, with most provinces forming either high-pollution clusters or low-pollution clusters [5]. This suggests that interregional interactions should be considered in pollution assessment. For dynamic analysis, the spatial Markov chain has been introduced to characterize transitions in regional pollution levels and their spatial dependence over time [13]. Unlike the traditional Markov chain, the spatial Markov chain incorporates a spatial weight matrix so that neighboring states can influence transition probabilities, overcoming the assumption of independent regional evolution [14]. Recent studies have increasingly combined the Dagum Gini coefficient, kernel density estimation, Moran's I, and spatial Markov chains to examine regional disparities and dynamic evolution in agricultural green development and pollution indicators, providing useful tools for integrated spatiotemporal analysis.

Despite these advances, important gaps remain. First, many studies are constrained by limited time spans or spatial coverage: some focus on specific provinces or regions and lack national comparability, while others use national data ending relatively early and cannot capture recent changes in pollution loads or management outcomes [8]. Second, prior research often emphasizes only one dimension – spatial patterns, distributional disparities, or temporal trends – while relatively few studies integrate multiple methods to jointly analyze spatial imbalance, distributional evolution, and spatial dynamics. In response, this study uses updated provincial data for 2017-2024 to conduct a comprehensive assessment of agricultural non-point source pollution loads in China. Specifically, we combine Dagum Gini decomposition to identify regional disparities and their sources, kernel density estimation to track distributional changes, global and local Moran's I to test spatial dependence, and spatial Markov chains to model spatially conditioned state transitions. By integrating these methods, this study addresses limitations in temporal coverage and methodological breadth in the existing literature and, from the perspective of the nexus between straw resource utilization and agricultural non-point source pollution control, systematically reveals the spatiotemporal evolution and spatial differentiation of provincial pollution loads in China.

Materials and Methods

Data Sources

This study takes 31 provincial-level administrative units in mainland China, including provinces, autonomous regions, and municipalities, as the observation units, and systematically estimates and analyzes the agricultural non-point source pollution effects associated with crop straw fertilizer utilization since the implementation of the Rural Revitalization Strategy. The study period spans 2017-2024. The underlying data are mainly drawn from the China Statistical Yearbook (2018-2025) and the China Rural Statistical Yearbook (2018-2025). Because yearbooks compile statistical information for the corresponding year, to ensure consistency and comparability of the time series, this study follows the official statistical definitions and compiles the basic indicators into a provincial panel dataset, which is then used for subsequent pollution accounting and spatiotemporal analyses.

The analysis focuses on non-point source pollution loads generated during crop straw fertilizer utilization and selects total nitrogen (TN), total phosphorus (TP), and chemical oxygen demand (COD) as the core pollutant indicators. This selection is based on three considerations. First, TN and TP are the principal nutrient pollutants in agricultural non-point source pollution and are directly related to nutrient runoff, water quality deterioration, and eutrophication risk. Second, COD reflects the oxygen-consuming pressure caused by the release, transport, and decomposition of straw-derived organic matter, and therefore complements TN and TP by capturing the organic pollution dimension of straw fertilizer utilization. Third, TN, TP, and COD are widely used in agricultural non-point source pollution accounting and environmental policy evaluation in China, which improves both the comparability of this study with existing literature and the practical relevance of the results for pollution-control policy.

Because the present study aims to estimate source-specific pollution loads attributable to crop straw fertilizer utilization rather than total agricultural emissions from all sources, the combined use of TN, TP, and COD provides a focused and policy-relevant indicator system for representing both nutrient-related and organic environmental risks. In addition, no single analytical tool can simultaneously reveal pollution-load levels, regional inequality, distributional evolution, spatial dependence, and dynamic transition characteristics. Therefore, this study combines pollution-load accounting with Dagum Gini decomposition, kernel density estimation, Moran's I, and spatial Markov chain analysis. Specifically, pollution-load accounting is used to quantify province-level pollution loads from crop straw fertilizer utilization; Dagum Gini decomposition is used to identify the magnitude and sources of regional disparities; kernel density estimation is used to describe distributional changes and tail characteristics; global and local Moran's I are used to test overall and local spatial association; and the spatial Markov chain is used to characterize state persistence and neighborhood-conditioned transition probabilities. This integrated framework is consistent with the objective of the study, namely, to depict the spatiotemporal evolution, regional heterogeneity, and spatial dynamic features of non-point source pollution loads from crop straw fertilizer utilization in China.

Accounting for Non-Point Source Pollution Loads

Based on the above indicator system, this study further estimates, for each province during 2017-2024, the pollution loads of total nitrogen (TN), total phosphorus (TP), and chemical oxygen demand (COD) associated with crop straw fertilizer utilization. The resulting provincial panel dataset serves as the basis for subsequent inequality decomposition, distributional dynamics, and spatial analyses. Major crops in China are included when estimating straw production, namely rice, wheat, maize, legumes, tubers, oil crops, and vegetables.

Let i denote province, t denote year, c denote crop type, and p denote pollutant type. The non-point source pollution load of pollutant p in province i and year t is defined as the sum of contributions across crop types:

$$NPS_{p,i,t} = \sum_{c} \left(Y_{c,i,t} \times \theta_c \times E_i \times \omega_{p,c} \times \delta_p \right)$$

where $NPS_{p,i,t}$ is the non-point source pollution load of pollutant p attributable to crop straw fertilizer utilization; $Y_{c,i,t}$ is the output of crop c in province i and year t; θ_c is the straw coefficient (straw-to-grain ratio) for crop c (Table 1), used to convert crop output to straw production; $\omega_{p,c}$ is the content parameter of pollutant p in the straw of crop c (Table 1); E_i is the provincial fertilizer utilization rate of crop straw (Table 2); and δ_p is the discharge coefficient of pollutant p. Specifically, δ_{TN}=15.00%, δ_{TP}=2.18%, and δ_{COD}=20.00%. All parameters used in the accounting are drawn from relevant domestic and international studies [15, 16].

Dagum Gini Coefficient and Decomposition

To characterize the overall level of interprovincial disparity in straw-related non-point source pollution

Table 1. Straw coefficients and pollutant contents in straw by crop type.

Crop type	Straw coefficient	Pollutant content/%		
		TN	TP	COD
Wheat	1.381	0.50	0.20	0.60
Rice	0.927	0.60	0.10	0.60
Maize	1.174	0.80	0.40	0.80
Legumes	1.508	1.30	0.30	1.00
Oil crop	2.331	2.00	0.30	1.00
Tubers	0.481	0.30	0.25	0.40
Vegetables	0.071	0.18	0.20	1.00

Table 2. Provincial fertilizer utilization rates of crop straw in China.

Province	Utilization rate (%)	Province	Utilization rate (%)
Anhui	30.30	Jilin	31.10
Fujian	35.50	Jiangsu	31.90
Gansu	26.80	Jiangxi	65.10
Guangdong	41.40	Liaoning	31.10
Guizhou	15.00	Ningxia	7.00
Hainan	38.00	Shandong	23.60
Hebei	47.30	Shanxi	55.70
Henan	34.60	Shaanxi	32.00
Heilongjiang	35.10	Shanghai	47.80
Hubei	38.00	Sichuan	14.30
Hunan	71.00	Zhejiang	23.90

Note: Provinces not listed in Table 2 adopt the national uniform fertilizer utilization rate of crop straw (36.60%).

loads during 2017-2024 and to further identify the sources of inequality, this study applies the Dagum Gini coefficient and its decomposition. Compared with conventional decomposition schemes, the Dagum approach partitions overall inequality into three components – within-group inequality, net between-group inequality, and transvariation intensity – making it particularly suitable when distributions overlap across groups [17]. Provinces are used as the basic observation units, and the sample is divided into G subgroups under a predetermined grouping rule (denoted $g = 1,...,G$); annual estimation and decomposition are conducted accordingly.

Let $x_{i,t}$ denote the non-point source pollution load of a given pollutant for province i in year t. Let the number of provinces be n, and the overall mean be $\mu_t = \frac{1}{n}\sum_{i=1}^{n} x_{i,t}$. After grouping, the sample size of group g is n_g, and the group mean is $\mu_{g,t} = \frac{1}{n_g}\sum_{i\in g} x_{i,t}$. The overall Dagum Gini coefficient is defined as:

$$G_t = \frac{1}{2n^2\mu_t}\sum_{i=1}^{n}\sum_{j=1}^{n} | x_{i,t} - x_{j,t} |$$

Here, $|x_{i,t}-x_{j,t}|$ is the absolute difference in pollution load between two provinces. The denominator $2n^2\mu_t$ standardizes the index by sample size and mean level, so that $G_t \in [0,1]$; larger values indicate greater interprovincial disparity. Under the grouping framework, the Dagum decomposition satisfies:

$$G_t = G_{w,t} + G_{nb,t} + G_{tv,t}$$

where $G_{w,t}$ is the within-group contribution, $G_{nb,t}$ is the net between-group contribution, and $G_{tv,t}$ is the transvariation (overlap) contribution.

The within-group component is a weighted sum of group-specific within-group Gini coefficients. For group g,

$$G_{g,t} = \frac{1}{2n_g^2\mu_{g,t}}\sum_{i\in g}\sum_{j\in g} | x_{i,t} - x_{j,t} |$$

Accordingly,

$$G_{w,t} = \sum_{g=1}^{G}\left(\frac{n_g}{n}\right)^2\left(\frac{\mu_{g,t}}{\mu_t}\right)G_{g,t}$$

This expression uses two weights: $\left(\frac{n_g}{n}\right)^2$ reflects the share of within-group pairings, and $\left(\frac{\mu_{g,t}}{\mu_t}\right)$ reflects the group's relative pollution level in the overall distribution, ensuring that both sample size and pollution level are considered.

For any two groups g and $h(g\neq h)$, define the average absolute difference ("between-group distance") as:

$$D_{gh,t} = \frac{1}{n_g n_h}\sum_{i\in g}\sum_{j\in h} | x_{i,t} - x_{j,t} |$$

To separate "between-group differences driven purely by mean gaps" from differences caused by distributional overlap, the Dagum method further decomposes pairwise differences into positive and reverse components. Without loss of generality, assume $\mu_{h,t} \geq \mu_{g,t}$, and define:

$$d_{gh,t} = \frac{1}{n_g n_h}\sum_{i\in g}\sum_{j\in h} \max\left(0, x_{j,t} - x_{i,t}\right)$$

$$p_{gh,t} = \frac{1}{n_g n_h}\sum_{i\in g}\sum_{j\in h} \max\left(0, x_{i,t} - x_{j,t}\right)$$

Here, $d_{gh,t}$ is the average "forward" difference when observations in the higher-mean group h exceed those in group g, whereas $p_{gh,t}$ captures the average "reverse" difference (reflecting overlap). By definition,

$$D_{gh,t} = d_{gh,t} + p_{gh,t}$$

and the difference between forward and reverse components equals the mean gap:

$$d_{gh,t} - p_{gh,t} = \mu_{h,t} - \mu_{g,t}$$

Based on these relationships, the net between-group contribution and transvariation contribution are expressed as:

$$G_{nb,t} = \sum_{g=1}^{G-1}\sum_{h=g+1}^{G}\frac{n_g n_h}{n^2\mu_t}\left(\mu_{h,t} - \mu_{g,t}\right)$$

$$G_{tv,t} = \sum_{g=1}^{G-1}\sum_{h=g+1}^{G}\frac{n_g n_h}{n^2\mu_t}\left(2p_{gh,t}\right)$$

The first term reflects the role of between-group mean gaps, while the second term captures the contribution of distributional overlap across groups.

Kernel Density Estimation

To describe, from a continuous-distribution perspective, the distributional shape and evolution of provincial straw-related non-point source pollution loads since the Rural Revitalization Strategy (2017-2024), this study applies kernel density estimation (KDE) to the cross-sectional sample of 31 provinces in each year [18]. Compared with discrete grouping methods (e.g., histograms), KDE does not impose a parametric distribution and provides a smoothed representation of concentration, skewness, tail behavior, and potential multimodality. This allows more intuitive identification of distributional shifts (upward or downward), changes in dispersion, and possible polarization.

Let $x_{i,t}$ denote the pollution load of a given pollutant for province i in year t(unit: 10^4 tons), and let n = 31. The KDE for year t is:

$$\hat{f}_t(x) = \frac{1}{nh_t}\sum_{i=1}^{n}K\left(\frac{x - x_{i,t}}{h_t}\right)$$

where $\hat{f}_t(x)$ is the estimated density at x; $K(\cdot)$ is the kernel function (a Gaussian kernel is used); and h_t>0 is the bandwidth parameter controlling smoothness. A large bandwidth may over-smooth the curve and mask distributional details, whereas a small bandwidth can produce excessive fluctuations and reduce interpretability. Given the limited cross-sectional sample size and the possibility of skewness and extreme values, Silverman's rule of thumb is adopted to determine h_t, improving robustness and ensuring comparability across years:

$$h_t = 0.9 \cdot \min\left(\sigma_t, \frac{\mathrm{IQR}_t}{1.34}\right) \cdot n^{-1/5}$$

where σ_t is the standard deviation in year t, $IQR_t = Q_{75,t} - Q_{25,t}$ is the interquartile range, and $IQR_t/1.34$ serves as a robust alternative to the standard deviation to reduce sensitivity to extreme values.

Spatial Autocorrelation Analysis

Specification of the Spatial Weight Matrix

Spatial statistical analysis requires a spatial weight matrix $W = [w_{ij}]$ to represent spatial adjacency and potential interactions between provinces i and j. This study constructs a contiguity-based provincial adjacency matrix: $w_{ij} = 1$ if provinces i and j share a common border, and $w_{ij} = 0$ otherwise; diagonal elements are set to $w_{ii} = 1$. To interpret the spatial lag as a neighborhood average, the matrix is row-standardized:

$$w_{ij}^{*} = \frac{w_{ij}}{\sum_{j=1}^{n} w_{ij}}$$

where $n = 31$. After row standardization, the weights in each row sum to 1. The spatial lag term $Wx_{i,t} = \sum_j w_{ij}^{*} x_{j,t}$ can thus be interpreted as the weighted average pollution level of provinces adjacent to province i.

Global Spatial Autocorrelation

Global Moran's I is used to test whether provincial pollution loads exhibit overall spatial clustering. For year t, Moran's I is defined as:

$$I_t = \frac{n}{S_0} \cdot \frac{\sum_{i=1}^{n} \sum_{j=1}^{n} w_{ij}^{*} \left(x_{i,t} - \bar{x}_t\right)\left(x_{j,t} - \bar{x}_t\right)}{\sum_{i=1}^{n} \left(x_{i,t} - \bar{x}_t\right)^2}$$

where $\bar{x}_t = \frac{1}{n} \sum_{i=1}^{n} x_{i,t}$ is the provincial mean in year t, and $S_0 = \sum_{i=1}^{n} \sum_{j=1}^{n} w_{ij}^{*}$ is the sum of all weights. When $I_t > 0$, similar values tend to cluster (High–High or Low–Low adjacency); when $I_t < 0$, dissimilar values tend to be adjacent; and when I_t is close to 0, overall clustering is weak. Statistical significance is assessed using a random permutation test: observed values are randomly permuted across provinces while keeping the set of values unchanged, Moran's I is recalculated repeatedly to form an empirical null distribution, and a p-value is obtained accordingly.

Local Spatial Autocorrelation

To identify local hotspot and coldspot patterns, local Moran's I(LISA) is used for local clustering diagnostics. For province i in year t, local Moran's I is defined as:

$$I_{i,t} = \frac{\left(x_{i,t} - \bar{x}_t\right)}{m_{2,t}} \sum_{j=1}^{n} w_{ij}^{*} \left(x_{j,t} - \bar{x}_t\right)$$

where, $m_{2,t} = \frac{1}{n} \sum_{i=1}^{n} (x_{i,t} - \bar{x}_t)^2$ is the variance term. Significance can likewise be evaluated via permutation tests. Based on the sign combination of the local statistic and standardized values, local spatial association is classified into "High–High", "Low–Low", "High–Low", and "Low–High" types, which helps identify potential pollution hotspots and spatial outliers.

Spatial Markov Chain Analysis

Building on the spatial autocorrelation assessment, a spatial Markov chain model is introduced to further characterize the dynamic evolution of straw-related non-point source pollution loads and to examine spatial conditioning effects. By combining the "state transition" framework of a traditional Markov chain with neighborhood information, the spatial Markov approach tests whether the probabilities of staying in the same pollution state, moving upward, or moving downward differ systematically under different neighborhood pollution contexts. This provides evidence on whether the interprovincial evolution of pollution loads is shaped by spatial dependence.

State Classification and Construction of Local State Variables

Let $x_{i,t}$ denote the pollution load of province i in year t. A quantile-based method is applied to divide the provincial sample in each year into four quartile states from low to high:

$$S_{i,t} \in \{1,2,3,4\}$$

For ease of interpretation, the four states are labelled LL, L, H, and HH, where $S_{i,t} = 1$ represents the lowest pollution level (LL) and $S_{i,t} = 4$ represents the highest pollution level (HH). Quartile classification ensures that state sizes remain relatively balanced even with a limited sample, improving the stability of transition probability estimation.

As a benchmark, the conventional (unconditional) Markov transition probability matrix is first estimated. For a one-year transition step:

$$p_{mn} = \Pr(S_{t+1} = n \mid S_t = m)$$

which forms a 4×4 unconditional transition matrix $P = [p_{mn}]$.

Construction of Neighborhood State Variables

The defining feature of the spatial Markov chain is to condition transitions on neighborhood context. Based on the row-standardized weight matrix $W = [w^{*}_{ij}]$, the spatial lag is constructed as:

$$Wx_{i,t} = \sum_{j=1}^{n} w_{ij}^{*} x_{j,t}$$

where $(Wx)_{i,t}$ represents the neighborhood pollution level of province i in year t. To align with the discretization of local states, the same quartile method is used to classify $(Wx)_{i,t}$ into four neighborhood states:

$$WState_{i,t} \in \{1,2,3,4\}$$

Estimation of Conditional Transition Probability Matrices

Conditional on neighborhood state k, the spatial Markov chain describes transitions of the local state. The conditional transition probability is:

$$p_{mn}^{(k)} = \Pr(S_{t+1} = n \mid S_t = m, WState_t = k, k \in \{1,2,3,4\}$$

Empirically, transition frequencies under $WState_{i,t} = k$ are counted:

$$n_{mn}^{(k)} = \#\{(i,t) \mid S_{i,t} = m, S_{i,t+1} = n, WState_t = k\}$$

and conditional transition probabilities are computed as:

$$p_{mn}^{(k)} = \frac{n_{mn}^{(k)}}{\sum_{n=1}^{4} n_{mn}^{(k)}}$$

This yields four 4×4 conditional transition matrices $P^{(k)} = [p_{mn}^{(k)}]$. Comparing diagonal probabilities with off-diagonal probabilities across different k helps evaluate whether neighborhood context alters the evolution tendency of local pollution states.

Summary Indicators for Staying, Upward, and Downward Transitions

Because cell-by-cell comparison of conditional matrices can be cumbersome, three summary indicators are constructed: staying, upward transitions, and downward transitions. For any neighborhood state k,

$$\text{Stay\_count}^{(k)} = \sum_{m=1}^{4} n_{mm}^{(k)}$$

$$\text{Up\_count}^{(k)} = \sum_{m=1}^{4} \sum_{n>m} n_{mn}^{(k)}$$

$$\text{Down\_count}^{(k)} = \sum_{m=1}^{4} \sum_{n<m} n_{mn}^{(k)}$$

The total number of transitions is:

$$N^{(k)} = \sum_{m=1}^{4} \sum_{n=1}^{4} n_{mn}^{(k)}$$

Accordingly, the probabilities are:

$$\text{Stay\_prob}^{(k)} = \frac{\text{Stay\_count}^{(k)}}{N^{(k)}}, \text{Up\_prob}^{(k)} = \frac{\text{Up\_count}^{(k)}}{N^{(k)}}, \text{Down\_prob}^{(k)} = \frac{\text{Down\_count}^{(k)}}{N^{(k)}}$$

Study Region Division

To characterize regional differences in straw-related non-point source pollution loads under different development stages and resource endowments, and to facilitate regional comparison and inequality decomposition, the 31 provincial-level units are divided into four major regions – Eastern, Central, Western, and Northeastern China – following a widely used regional classification in national statistics and regional studies [19]. This division maintains statistical consistency while reflecting the major structural differences across China's regions.

Specifically, the Eastern region includes Beijing, Tianjin, Hebei, Shanghai, Jiangsu, Zhejiang, Fujian, Shandong, Guangdong, and Hainan; the Central region includes Shanxi, Anhui, Jiangxi, Henan, Hubei, and Hunan; the Western region includes Inner Mongolia, Guangxi, Chongqing, Sichuan, Guizhou, Yunnan, Tibet, Shaanxi, Gansu, Qinghai, Ningxia, and Xinjiang; and the Northeastern region includes Liaoning, Jilin, and Heilongjiang.

Results

Annual Trends in National Non-point Source Pollution Loads from Crop Straw Fertilizer Utilization

At the national level, non-point source pollution loads from crop straw fertilizer utilization showed an overall upward trend during 2017-2024, with faster growth in the later years. The three pollutants followed a similar pattern: slight decline or near stability in 2017-2018, a shift to growth after 2019, and clearer increases during 2022-2024 (Fig. 1). For total nitrogen (TN), the estimated load increased from 35.02 to 38.82 (10^4 t), an absolute increase of 3.80 (10^4 t) (10.85%). TN declined slightly from 35.02 to 34.87 (10^4 t) in 2017-2018, then rose continuously after 2019, with relatively larger annual increments in 2022-2024. This indicates a continued accumulation of nitrogen-related pollution loads alongside the expansion or adjustment of straw fertilizer utilization. Total phosphorus (TP) remained

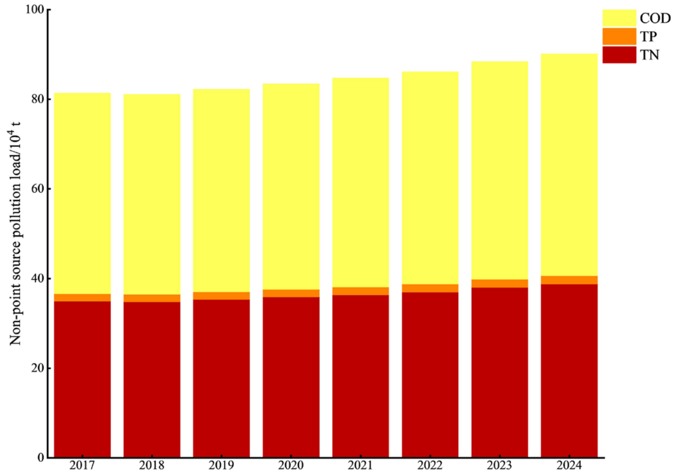

Fig. 1. Total non-point source pollution loads from crop straw fertilizer utilization in China, 2017-2024.

much smaller than TN and COD in absolute magnitude, but also increased steadily. It rose from 1.68 to 1.88 (10^4 t) during 2017-2024, an increase of 0.20 (10^4 t). After minor fluctuations in 2017-2018, TP increased year by year, suggesting a parallel rise in phosphorus-related pollution risk nationwide, although the absolute increase was moderate. Chemical oxygen demand (COD) was the largest pollutant throughout the period and also increased substantially, from 44.60 to 49.33 (10^4 t), with an absolute increase of 4.73 (10^4 t). Similar to TN, COD declined slightly in 2017-2018 (44.60 to 44.44 (10^4 t)) and then increased continuously after 2019, with relatively strong growth in 2023-2024. This suggests a clear scale effect in pollution loads associated with organic matter release during straw fertilizer utilization.

Interprovincial Disparities and Source Decomposition

Table 3 highlights two core features of the provincial distribution: interprovincial inequality remained persistently high throughout 2017-2024, and between-region differences consistently contributed more to overall disparity than within-region differences. The overall Gini coefficient ranged from 0.509 to 0.517, indicating persistent and visible interprovincial disparities in pollution loads throughout the study period. Temporally, the overall Gini was 0.514 in 2017, rose slightly to 0.516~0.517 during 2018-2020, and then gradually declined to 0.509 in 2024. Although the change was small, interprovincial inequality weakened marginally in the later years. Decomposition results show that overall inequality was driven mainly by between-region differences. The between-group component (G_b) ranged from 0.276 to 0.289 and remained consistently higher than the within-group component (G_w, 0.103~0.105), indicating that regional differences in average pollution-load levels contributed more to total inequality than disparities within regions. G_b declined gradually from 0.289 in 2017 to 0.276 in 2024, suggesting a slow narrowing of regional gaps, although they remained the dominant source of inequality. Within-group inequality was largely stable. G_w varied only slightly (0.103~0.105), implying no pronounced expansion or contraction of disparities within regions during 2017-2024. By region, the Eastern region had the highest within-group Gini, indicating the largest internal disparities. The Western region ranked second

Table 3. Gini coefficient of total non-point source pollution loads from crop straw fertilizer utilization in China.

Year	Total	G_w	G_b	G_t	Eastern	Central	Western	Northeastern
2017	0.514	0.103	0.289	0.122	0.620	0.237	0.447	0.241
2018	0.516	0.105	0.288	0.124	0.615	0.244	0.455	0.265
2019	0.517	0.105	0.286	0.125	0.615	0.248	0.463	0.245
2020	0.517	0.105	0.288	0.124	0.615	0.251	0.459	0.253
2021	0.513	0.104	0.285	0.124	0.613	0.241	0.460	0.239
2022	0.514	0.104	0.286	0.124	0.611	0.245	0.458	0.246
2023	0.510	0.104	0.281	0.125	0.608	0.240	0.465	0.240
2024	0.509	0.105	0.276	0.128	0.609	0.241	0.467	0.246

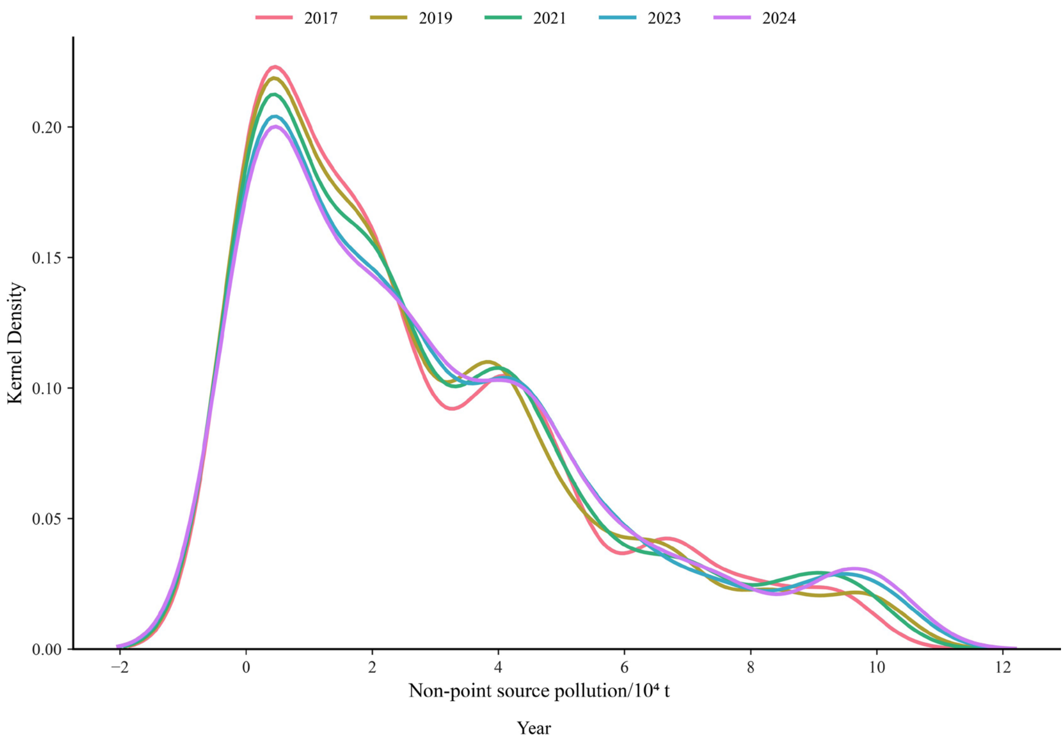

Fig. 2. Kernel density curves of non-point source pollution loads from crop straw fertilizer utilization.

and increased from 0.447 in 2017 to 0.467 in 2024, suggesting widening internal differences. In contrast, the Central and Northeastern regions had lower within-group Gini coefficients, indicating relatively smaller internal disparities. The transvariation component (G_t) ranged from 0.122 to 0.128 and increased slightly in the later years (0.128 in 2024). This suggests persistent overlap in interregional distributions: some provinces in different regions had similar pollution-load levels, so regional classification alone could not fully separate overall disparities. Taken together, the modest decline in total inequality appears to be mainly associated with narrowing between-region gaps, while within-region disparities and distributional overlap changed only slightly.

Interprovincial Distribution and its Changes

Fig. 2 shows kernel density curves of provincial pollution loads for 2017, 2019, 2021, 2023, and 2024. The curves are broadly similar across years and exhibit a clear right-skewed distribution: density is concentrated in the low-value range and gradually declines toward a long right tail. This indicates that most provinces remained at relatively low pollution-load levels, while a small number stayed at higher levels and extended the upper tail. Across all years, the distribution has a

Table 4. Global spatial autocorrelation test results (global Moran's *I*) for non-point source pollution loads from crop straw fertilizer utilization, 2017-2024.

Year	Adjacency matrix			Economic-geographic nested matrix		
	Moran's *I*	z-value	p-value	Moran's *I*	z-value	p-value
2017	0.013	0.389	0.349	-0.149	-1.267	0.103
2018	0.022	0.469	0.320	-0.153	-1.307	0.096
2019	0.021	0.459	0.323	-0.151	-1.285	0.099
2020	0.021	0.458	0.324	-0.155	-1.324	0.093
2021	0.021	0.462	0.322	-0.149	-1.261	0.104
2022	0.021	0.460	0.323	-0.152	-1.298	0.097
2023	0.032	0.554	0.290	-0.152	-1.299	0.097
2024	0.029	0.529	0.298	-0.152	-1.300	0.097

pronounced main peak in the low-value range, indicating that low-load provinces consistently accounted for a large share of the sample. From 2017 to 2024, however, the main peak became slightly lower and wider, implying a modest decline in low-value concentration and a broader spread into the low-to-medium range. In addition, a secondary peak or shoulder around 3~4 (10^4 t) appears in most years, suggesting a mild layered structure with a subset of provinces remaining at medium load levels. At the high end, the right tail around 9~10 (10^4 t) is thicker in 2023 and 2024 than in earlier years, indicating that high-load provinces became somewhat more prominent in the later period and may have experienced load accumulation.

Results of Global Spatial Autocorrelation Tests

Table 4 shows that the main conclusion is robust to alternative spatial weight matrices: regardless of matrix specification, global spatial dependence remains weak and statistically insignificant at the national scale. To test whether the conclusion on global spatial autocorrelation is sensitive to the specification of the spatial weight matrix, this study re-estimated the global Moran's I using an economic–geographic nested matrix in addition to the baseline adjacency matrix. As shown in Table 4, the sign and magnitude of Moran's I differ to some extent across the two matrices, but the overall conclusion remains unchanged: no statistically significant global spatial clustering is observed at the national level during 2017-2024. Under the adjacency matrix, Moran's I is positive in all years, ranging from 0.013 to 0.032, with z-values between 0.389 and 0.554 and p-values consistently above 0.10 (0.290-0.349). This indicates only a weak positive spatial association tendency among geographically adjacent provinces, which is not statistically significant. Moreover, the year-to-year variation is small. Although Moran's I shows a slight increase in 2023–2024 (0.032 and 0.029, respectively), the strength of spatial dependence remains too weak to support a significant global clustering pattern. Under the economic–geographic nested matrix, Moran's I is negative in all years, ranging from −0.155 to −0.149, with z-values from −1.324 to −1.261 and p-values between 0.093 and 0.104, i.e., close to but not consistently below the 10% significance level. This suggests a weak negative spatial association tendency (spatial dispersion/mismatch) when both economic linkages and geographic proximity are jointly considered. In other words, provinces with relatively high pollution loads are not necessarily surrounded by economically and geographically connected provinces with similarly high loads; instead, heterogeneous neighboring relationships may exist. This pattern implies that the spatial distribution of non-point source pollution loads from straw fertilizer utilization is shaped not only by geographic proximity, but also by differences in cropping structure, resource endowment, utilization practices, and regional governance capacity, which jointly weaken homogeneous clustering at the national scale.

Overall, the alternative-matrix robustness test supports the central conclusion of this study that global spatial dependence is weak and that local spatial pattern identification is more informative. Although the choice of spatial weight matrix affects the sign and numerical value of Moran's I (weakly positive under the adjacency matrix versus weakly negative under the economic–geographic nested matrix), the lack of strong statistical significance under both specifications indicates that the main conclusion does not rely on a single matrix setting. Therefore, subsequent analyses of local spatial heterogeneity (LISA) and spatial dynamic evolution (spatial Markov chain) remain necessary and substantively meaningful.

Patterns of Local Spatial Autocorrelation

Although the global Moran's I statistics do not reach conventional significance levels, the local spatial autocorrelation results help identify whether a small number of provinces exhibit relatively stable local clustering or local outlier patterns (Fig. 3). Based on the LISA cluster maps and corresponding significance tests for 2017, 2019, 2021, and 2024, most provinces are "not significant" in each year. This is consistent with the global results and indicates no clear pattern of large contiguous clusters at the national scale. At the same time, a small number of provinces show relatively stable local types across years.

First, the High–High (H–H) type shows notable stability. From 2017 to 2024, Anhui is consistently classified as H–H and statistically significant in each reported year. Fujian, Shandong, and Hubei also remain significant H–H provinces across the four years. This indicates that these provinces had relatively high pollution loads and were surrounded by provinces with similarly high loads, forming a stable local pattern of "high values next to high values". It should be emphasized that this reflects spatial co-location rather than causal interprovincial influence.

Second, the Low–Low (L–L) type is relatively concentrated in the southwest and is also stable. Sichuan and Yunnan are consistently classified as L–L and statistically significant in 2017, 2019, 2021, and 2024, suggesting that both provinces and their neighbors remained at relatively low pollution-load levels.

Third, the Low–High (L–H) type mainly reflects local outliers. Shanxi is consistently classified as L–H and statistically significant in all four years, indicating comparatively low local loads but relatively high neighboring loads. In practical terms, such provinces merit attention because they are embedded in higher-load surroundings, although whether substantive spillover or transmission exists requires further evidence from the dynamic analysis.

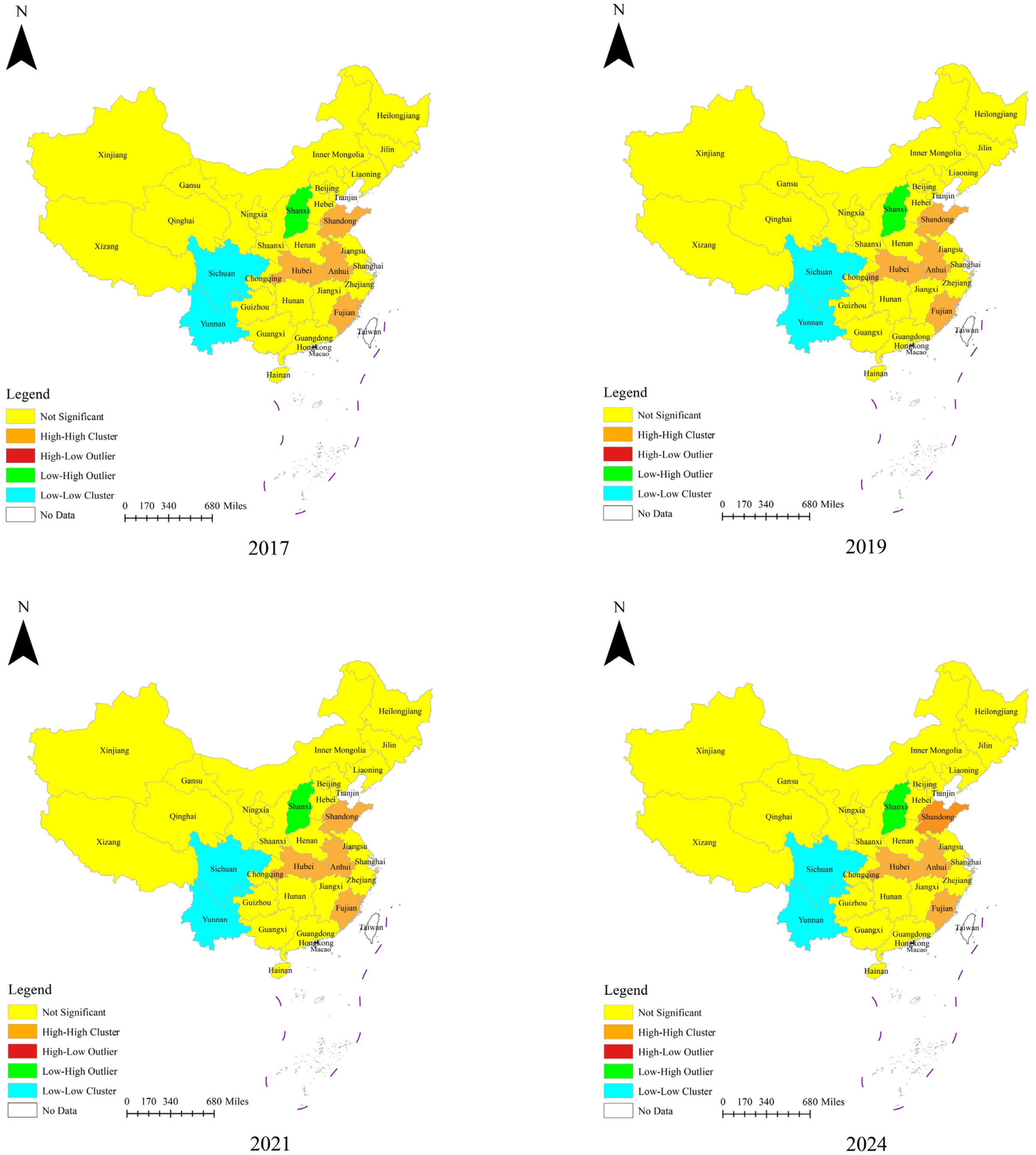

Fig. 3. Local spatial autocorrelation clustering distribution of non-point source pollution from straw fertilizer utilization in 2017, 2019, 2021, and 2024.

State Transitions under Different Neighborhood Conditions

Tables 5 and 6 jointly show that provincial pollution states are characterized by strong persistence, while high-neighborhood contexts are associated with relatively more active upward transitions among medium-to-high load provinces. As shown in Table 5, all neighborhood-conditioned transition matrices exhibit clear diagonal dominance, meaning that the probability of remaining in the same local state is generally high. This indicates strong persistence in provincial pollution states from one year to the next. Under an LL neighborhood context, for example, the probabilities of remaining in LL, L, and H are 0.964, 0.909, and 1.000, respectively. Similarly, under L or H neighborhood contexts, staying probabilities for LL, L, and H are mostly within 0.923~1.000. Overall, provincial pollution levels changed infrequently during 2017-2024, and most changes were small adjustments around existing levels.

The summary results in Table 6 confirm this pattern. Across the four neighborhood contexts, staying probabilities are 0.964 (LL), 0.981 (L), 0.981 (H), and 0.925 (HH), all substantially higher than upward and

Table 5. Conditional transition probability matrices of pollution states under different neighborhood contexts.

Neighborhood type	Local state	LL	L	H	HH
LL	LL	0.964	0.036	0.000	0.000
	L	0.000	0.909	0.091	0.000
	H	0.000	0.000	1.000	0.000
	HH	0.000	0.000	0.000	0.000
L	LL	0.923	0.077	0.000	0.000
	L	0.000	1.000	0.000	0.000
	H	0.000	0.000	1.000	0.000
	HH	0.000	0.000	0.000	1.000
H	LL	1.000	0.000	0.000	0.000
	L	0.000	1.000	0.000	0.000
	H	0.000	0.000	0.667	0.333
	HH	0.000	0.000	0.000	1.000
HH	LL	0.000	0.000	0.000	0.000
	L	0.000	0.000	0.000	0.000
	H	0.000	0.000	0.885	0.115
	HH	0.000	0.000	0.037	0.963

Table 6. Summary of transition directions and probabilities under spatial conditioning.

Neighborhood type	Number of transitions	Stay count	Upward count	Downward count	Stay probability	Upward probability	Downward probability
LL	56	54	2	0	0.964	0.036	0.000
L	54	53	1	0	0.981	0.019	0.000
H	54	53	1	0	0.981	0.019	0.000
HH	53	49	3	1	0.925	0.057	0.019

downward transition probabilities. Thus, regardless of neighborhood context, one-year state evolution is dominated by persistence. Table 6 also shows that upward transition probabilities exceed downward probabilities in all four neighborhood types, while downward transitions are zero under LL, L, and H contexts. This suggests that downward movements were rare in the observed transitions. By contrast, upward probabilities are 0.036, 0.019, and 0.019 under LL, L, and H neighborhoods, respectively, indicating occasional upward shifts even in low- to medium-neighborhood contexts.

Under the HH neighborhood context, the upward probability increases to 0.057, and a non-zero downward probability appears (0.019). Combined with Table 5, under HH neighborhoods a province in state H has a 0.333 probability of moving up to HH. Provinces already in HH remain highly persistent (0.963), but still have a 0.037 probability of moving down to H. This indicates that state transitions among higher-load provinces become more active under high-neighborhood conditions, with upward shifts being more common, although some downward adjustment is also present.

A comparison of key transitions across neighborhood types further suggests that neighborhood effects are more pronounced for higher states (H and HH). Under LL neighborhoods, the local H state is fully persistent (1.000). Under H neighborhoods, the staying probability of the local H state declines to 0.667 and the probability of moving up to HH rises to 0.333. Under HH neighborhoods, the staying probability of the local H state is 0.885, with a continuing probability of moving up to HH (0.115). These results indicate that when neighboring provinces are at relatively high pollution levels, provinces already in medium-to-high states are more likely to move upward.

Discussion

This study shows that China's non-point source pollution loads associated with crop straw fertilizer utilization increased slowly during 2017-2024, with COD accounting for the largest share and TP the smallest. This pollutant structure is closely related to the material characteristics of straw itself: the expansion of straw return and related fertilizer utilization increases organic matter inputs to cropland, thereby making COD the dominant component, whereas the relatively low phosphorus content in straw constrains TP loads [20]. At the same time, the observed upward trend should be interpreted as source-specific evidence rather than as a contradiction of broader studies reporting stabilization or decline in overall agricultural non-point source pollution intensity [21]. Many macro-level studies evaluate multiple pollution sources and longer time spans and are therefore more likely to capture the effects of fertilizer reduction, pesticide control, and livestock pollution management. By contrast, the present study isolates crop straw fertilizer utilization as one specific pathway under the Rural Revitalization period [21]. This distinction is important from a policy perspective, because it suggests that progress in controlling some agricultural pollution sources does not automatically imply simultaneous decline in all source-specific environmental risks.

Importantly, straw fertilizer utilization involves both environmental benefits and environmental risks. When properly managed, it can increase soil organic matter, improve nutrient-use efficiency, and reduce chemical fertilizer demand and nutrient losses [22, 23]. For example, in double-rice systems, optimized fertilization combined with straw incorporation reduced N and P losses in surface runoff by about 20.1% and 11.5%, respectively, without yield loss [24]. Therefore, the observed increase in total loads does not negate the ecological value of straw utilization; rather, it underscores the importance of improving management practices so that the benefits of straw return can be realized more consistently and at lower pollution risk.

The provincial distribution of straw-related pollution loads is highly uneven, and the Dagum decomposition shows that between-region differences are the dominant source of total inequality, while the Eastern region exhibits the largest within-region disparity. This pattern is closely related to interprovincial heterogeneity in agricultural production structure, cultivated scale, and resource endowment. In the East, major grain-producing provinces such as Shandong and Jiangsu generate large volumes of straw and sustain relatively intensive agricultural production, whereas municipalities or coastal provinces such as Shanghai and Hainan have much smaller agricultural sectors and lower straw-related load bases. As a result, high-load and low-load provinces coexist within the same region, widening internal disparities [25]. This interpretation is broadly consistent with the wider literature showing pronounced regional differentiation in agricultural emissions and environmental pressures [26], but our results further indicate that internal heterogeneity within economically advanced regions deserves more policy attention than simple east-west comparisons. The kernel density results reinforce this conclusion by showing a persistent right-skewed distribution and a long high-load tail, which implies that a limited number of provinces account for a disproportionate share of total loads. Therefore, regionally differentiated governance should combine broad regional strategies with more targeted intervention for provinces located in the high-load tail [25].

At the national scale, global Moran's I is not statistically significant, indicating weak overall spatial autocorrelation in straw-related pollution loads. However, this should not be interpreted as an absence of spatial structure. Local Moran's I still identifies relatively stable hotspot and coldspot provinces, indicating that source-specific pollution loads can display meaningful local clustering even when a nationwide clustering signal is weak. One reason is that crop straw fertilizer utilization depends strongly on cropping systems, crop composition, straw output, and local agronomic practices, which are unevenly distributed across China. Another reason is heterogeneity in policy implementation and governance capacity: provinces may respond differently to straw-return promotion, agricultural green development programs, and non-point source pollution control requirements. As a result, high-load provinces are not necessarily arranged in one large contiguous belt but may instead form several relatively independent local clusters. Compared with studies based on broader agricultural pollution indicators and longer time windows, this source-specific and shorter-period framework is therefore more likely to reveal weak global dependence but persistent local structure. From a governance perspective, the key implication is that place-based intervention remains necessary even when global spatial statistics are not significant.

The spatial Markov results indicate strong state persistence and show that neighborhood context is associated with transition probabilities. Across neighborhood types, the probability of remaining in the same state is consistently high, implying limited cross-state movement and relatively small year-to-year fluctuations. This is consistent with evidence that agricultural non-point source pollution categories tend to be stable over time [21], and with related spatial studies of agricultural carbon emission intensity showing persistent high- and low-state areas [26]. Such persistence likely reflects shared resource endowments, production structures, and policy environments among neighboring provinces, which can sustain stable clusters of environmental performance. From a governance perspective, this implies that breaking persistent high-load patterns requires coordinated regional intervention rather than isolated provincial action. If only one high-load province acts while neighboring provinces do not, the probability of shifting to a lower state may remain limited. By contrast, coordinated action across clustered high-load areas is more likely to change transition probabilities and reduce persistence.

Taken together, the present findings contribute to the broader literature by showing that environmental effects of straw resource utilization are not one-dimensional. Crop straw fertilizer utilization remains an important pathway for reducing open burning, recycling nutrients, and supporting green agricultural development, but its environmental performance depends strongly on management quality and regional conditions. In this sense, the policy challenge is not whether straw should be utilized, but how it should be utilized under different production structures, ecological constraints, and governance capacities. The source-specific perspective adopted here therefore complements broader intensity-based studies by revealing that short-term increases in one pollution source may coexist with overall improvement in aggregate agricultural pollution indicators.

Second, pronounced regional disparities imply that pollution control should move beyond uniform promotion targets and adopt more differentiated and targeted governance arrangements. High-load provinces face greater environmental pressure and should receive priority support. These provinces often have both large straw outputs and high utilization rates, and may benefit most from technical and financial support for improved processing and utilization technologies (e.g., higher-quality organic fertilizer production or bioenergy pathways) to reduce direct field loading. By contrast, low-load provinces – often economically developed areas with smaller agricultural shares – should consolidate gains and share management experience. Given the large internal disparities within the Eastern region, regional cooperation mechanisms are also needed, including coordinated programs and technology diffusion from better-performing provinces to neighboring high-load provinces.

Finally, local clustering patterns and spatial Markov results highlight the need for cross-boundary joint prevention and control. High–high clusters may span provincial borders, especially in contiguous grain-producing areas, making basin- or regional-scale coordination more effective than fragmented governance. Policy design could include coordinated mitigation targets, ecological compensation, earmarked green-development transfers, and stronger technical support to alter transition probabilities in persistent high-load areas. Prior evidence suggests that even after considering spatial effects, provincial pollution levels tend to remain stable with only small fluctuations, implying that major improvements in regional imbalance are unlikely without policy intervention [26]. At the same time, stable Low–Low clusters indicate that some regions have formed a virtuous cycle and can serve as demonstration zones for broader diffusion of effective management practices.

Limitations and Future Research Directions

Several limitations should be noted. First, this study is designed as a source-specific spatiotemporal pattern analysis of pollution loads from crop straw fertilizer utilization, rather than a determinant-oriented econometric investigation. Accordingly, the analysis focuses on load accounting, regional disparity decomposition, spatial association, and neighborhood-conditioned dynamic transitions, but does not estimate the marginal effects of economic development, agricultural production structure, cropping intensity, or environmental policy implementation on pollution loads. These factors are nonetheless important for explaining interprovincial heterogeneity [27]. Future research can build on the present framework by introducing richer explanatory variables and applying spatial panel models (e.g., SAR, SEM, or SDM) to examine the driving mechanisms and policy effects more explicitly.

Second, the pollution-load estimates depend on parameter assumptions (e.g., pollutant content and discharge coefficients). In the present study, these parameters mainly act as scaling terms within the accounting framework. We therefore focus on pattern identification rather than full uncertainty propagation. Although this choice does not alter the core contribution of the paper, future work should incorporate finer-scale parameter uncertainty (especially province- and crop-specific coefficients) and apply scenario-based or Monte Carlo sensitivity analysis to assess uncertainty bounds more comprehensively [28].

Third, the interpretation of spatial dependence is affected by indicator definition, time window, and spatial weight matrix specification. This study has added an alternative matrix robustness check and finds that the core conclusion – weak global spatial dependence but meaningful local structure – remains unchanged. However, different matrix constructions may still alter the sign or magnitude of global Moran's I [29]. Future studies can compare additional matrix forms (e.g., distance-based, k-nearest-neighbor, or flow-based matrices) to better represent interprovincial interactions relevant to straw utilization and pollution transport.

Finally, this study focuses on pollution loads associated with crop straw fertilizer utilization and does not directly compare all straw utilization pathways (e.g., feed, fuel, industrial uses) within one unified framework. As a result, the findings should be interpreted as source-specific evidence rather than a complete assessment of all straw-related environmental impacts. Future research should integrate multiple straw utilization pathways and jointly evaluate trade-offs among air pollution mitigation, water-environment risks, and resource efficiency [30].

Conclusions

This study examined the spatiotemporal evolution of non-point source pollution loads from crop straw fertilizer utilization in China during 2017-2024 using an integrated analytical framework. The results show that national pollution loads increased slowly over the study period, with COD contributing the largest load, followed by TN, while TP remained comparatively small. Interprovincial disparities remained pronounced, and overall inequality was driven mainly by between-region differences, although regional gaps narrowed slightly over time. The provincial distribution remained right-skewed, with most provinces concentrated at low load levels and a limited number of provinces forming a persistent high-load tail. Global spatial autocorrelation was weak and statistically insignificant under both the adjacency matrix and the economic–geographic nested matrix, indicating no strong nationwide clustering. However, local spatial analysis identified stable hotspot and coldspot provinces, and the spatial Markov results further showed strong state persistence, with neighborhood context affecting transition probabilities, especially for provinces in medium-to-high pollution states. Overall, the findings indicate that crop straw fertilizer utilization should be understood as a source-specific environmental issue: although it contributes to straw recycling and the reduction of open burning, its associated pollution pressures do not automatically decline in the short term. Therefore, policy efforts should combine straw resource utilization with improved agronomic management, differentiated regional governance, and cross-boundary coordination in locally clustered high-load areas.

Acknowledgements

This research was supported by the General Program of the National Social Science Fund of China, titled "Research on Multi-Dimensional Social Capital and the Cultivation Pathways for New Farmer Entrepreneurship Growth" (Grant No. 23BZZ063).

AI Usage Disclosure Statement

During the preparation of this work the authors used OpenAI ChatGPT-5.4 in order to assist in English language editing, grammatical correction and manuscript polishing. After using these tools, the authors reviewed and edited the content as needed and take full responsibility for the content of the published article.

Conflict of Interest

The authors declare no conflict of interest.

References

1. CHI H., ZHANG W., LIU Z., LIU X. Estimation of carbon emission reduction potential from fertilized utilization of crop straw in China. Journal of Shanxi Agricultural University(Natural Science Edition), **45** (5), 100, **2025**.
2. RANJAN A., KHANNA S., MOHOLKAR V.S. Feasibility of rice straw as alternate substrate for biobutanol production. Applied Energy, **103**, 32, **2013**.
3. GUO Z., LIU Y., MENG X., YANG X., MA C., CHAI H., LI H., DING R., NAZAROV K., ZHANG X., HAN Q. The long-term nitrogen fertilizer management strategy based on straw return can improve the productivity of wheat-maize rotation system and reduce carbon emissions by increasing soil carbon and nitrogen sequestration. Field Crops Research, **317**, 109561, **2024**.
4. WANG Y., LIANG B.Q., BAO H., CHEN Q., CAO Y.L., HE Y.Q., LI L.Z. Potential of crop straw incorporation for replacing chemical fertilizer and reducing nutrient loss in Sichuan Province, China. Environmental Pollution, **320**, 121034, **2023**.
5. HU J.H., XUE L.H., QIAN C., XUE L.X., CAO S. Effects of Aeration on Surface Water Nutrient Dynamics and Greenhouse Gas Emission in Different Straw Returning Paddy Fields. Environmental Science, **44** (4), 2348, **2023**.
6. WANG S., ZHAI L., GUO S., ZHANG F., HUA L., LIU H. Returned straw reduces nitrogen runoff loss by influencing nitrification process through modulating soil C:N of different paddy systems. Agriculture, Ecosystems & Environment, **354**, 108438, **2023**.
7. WANG Y., SHAN Q., WANG C., FENG S., LI Y. Research Progress and Application Analysis of the Returning Straw Decomposition Process Based on CiteSpace. Water, **15** (19), 3426, **2023**.
8. XU L., JIANG J., LU M., DU J. Spatial-Temporal Evolution Characteristics of Agricultural Intensive Management and Its Influence on Agricultural Non-Point Source Pollution in China. Sustainability, **15** (1), 371, **2023**.
9. WANG M., HUANG X., DONG Y., SONG Y., WANG D., LI L., QI X., LIN N. Spatiotemporal drivers of agricultural non-point source pollution: A case study of the Huang-Huai-Hai Plain, China. Journal of Environmental Management, **370**, 122606, **2024**.
10. SUN B., ZHANG L., YANG L., ZHANG F., NORSE D., ZHU Z. Agricultural non-point source pollution in China: causes and mitigation measures. Ambio, **41** (4), 370, **2012**.
11. YANG M., CHU J., LI Z., LIU X., YU F., SUN F. An Examination of Regional Variations in Pesticide Usage and Grain Yield in China Before and After the Double Reduction Policy's Adoption. Polish Journal of Environmental Studies, **32** (2), 1887, **2023**.
12. WU H., ZHENG X., ZHOU L., MENG Y. Spatial autocorrelation and driving factors of carbon emission density of crop production in China. Environmental Science and Pollution Research, **31** (18), 27172, **2024**.
13. YAN J., TANG Z., GUAN Y., XIE M., HUANG Y. Analysis of Measurement, Regional Differences, Convergence and Dynamic Evolutionary Trends of the Green Production Level in Chinese Agriculture. Agriculture, **13** (10), 2016, **2023**.
14. YU B., YANG X., WU X. Study on spatial spillover effects and influencing factors of carbon emissions in county areas of Ha-Chang city group: Evidence from NPP-VIIRS nightlight data. Acta Scientiae Circumstantiae, **40** (2), 697, **2020**.

15. CHEN T., LU J., LU T., YANG X., ZHONG Z., FENG H., WANG M., YIN J. Agricultural non-point source pollution and rural transformation in a plain river network: Insights from Jiaxing city, China. Environmental Pollution, **333**, 121953, **2023**.
16. LI C., CAI M., WANG X. Assessment and analysis of agricultural non-point source pollution loads in Henan, China: 2001-2023. PLoS One, **20**, (12), e0336116, **2025**.
17. MA T., LIU Y., YANG M. Spatial-Temporal Heterogeneity for Commercial Building Carbon Emissions in China: Based the Dagum Gini Coefficient. Sustainability, **14** (9), **2022**.
18. WANG N., QU Z., LI J., ZHANG Y., WANG H., XI H., GU Z. Spatial-temporal patterns and influencing factors of carbon emissions in different regions of China. Environmental Research, **276**, **2025**.
19. SU L., WANG Y., YU F. Analysis of regional differences and spatial spillover effects of agricultural carbon emissions in China. Heliyon, **9** (6), e16752, **2023**.
20. YANG S., WANG Y., LIU R., LI Q., YANG Z. Effects of straw application on nitrate leaching in fields in the Yellow River irrigation zone of Ningxia, China. Scientific Reports, **8** (1), 954, **2018**.
21. TIAN Y., XIA R., ZHANG X.Y. Evaluation of China's Agricultural Non-point Source Pollution Intensity: Spatial and Temporal Differentiation, Dynamic Evolution and Spatial Agglomeration. Environmental Science, **46** (9), 5608, **2025**.
22. XU L., CHEN H., ZHOU Y., ZHANG J., NADEEM M.Y., MIAO C., YOU J., LI W., JIANG Y., DING Y., LI G. Long-term straw returning improved soil nitrogen sequestration by accelerating the accumulation of amino acid nitrogen. Agriculture, Ecosystems & Environment, **362**, 108846, **2024**.
23. GUO J., JIANG P., ZHANG J., DONG S., TIAN W., LI J., LI F., LV J., YAO Y., HOU Y., WU S., SHAABAN M., HUANG M., LI Y. Straw Return Substituting Potassium Fertilizer Increases Crop Yield, Efficiency, and Quality in Maize-Wheat Rotation System. Agronomy, **14** (6), 1266, **2024**.
24. ZHANG Y., ZHU J., LI C., PENG H., LIU J., LUO Y., SONG M., DAI Y., DENG K., JI X. Optimizing fertilizer application and straw return to fields to minimize nitrogen and phosphorus runoff losses in double-rice cropping systems. Agricultural Water Management, **317**, 109601, **2025**.
25. LI S., ZHANG X., DENG Z., LIU K., WANG J., FAN J. Widening inequality: Diverging trends in CO2 and air pollutant emissions across Chinese cities. Resources, Environment and Sustainability, **21**, 100227, **2025**.
26. ZHU X., SHAO X. Spatiotemporal evolution of agricultural carbon emissions intensity in China and analysis of influencing factors. Scientific Reports, **15** (1), 19202, **2025**.
27. WANG H., LIU C., XIONG L., WANG F. The spatial spillover effect and impact paths of agricultural industry agglomeration on agricultural non-point source pollution: A case study in Yangtze River Delta, China. Journal of Cleaner Production, **401**, 136600, **2023**.
28. SHEN Z.-Y., HONG Q., YU H., NIU J.-F. Parameter uncertainty analysis of non-point source pollution from different land use types. Science of The Total Environment, **408**, (8), 1971, **2010**.
29. STAKHOVYCH S., BIJMOLT T.H.A. Specification of spatial models: A simulation study on weights matrices. Papers in Regional Science, **88** (2), 389, **2009**.
30. LI X., DU Y., CHANG H., AI J., ZHAO Y. Life cycle environmental impacts of five technological routes for straw utilisation in China. Biomass and Bioenergy, **183**, 107157, **2024**.